JVI Journals.ASM.org

Conformational Changes in Sindbis Virus Induced by Decreased pH Are Revealed by Small-Angle Neutron Scattering

Lilin He,[a,b] Amanda Piper,[c] Flora Meilleur,[b,c] Raquel Hernandez,[c] William T. Heller,[a,b] and Dennis T. Brown[c]

Center for Structural Molecular Biology, Oak Ridge National Laboratory, Oak Ridge, Tennessee, USA[a]; Neutron Scattering Sciences Division, Oak Ridge National Laboratory, Oak Ridge, Tennessee, USA[b]; and Department of Molecular and Structural Biochemistry, North Carolina State University, Raleigh, North Carolina, USA[c]

Alphaviruses, such as Sindbis virus, undergo dramatic changes in three-dimensional structure upon exposure to low pH, and such exposure can establish conditions allowing fusion of the virus membrane with a cell plasma membrane upon return to neutral pH. While exposure to low pH is not required for entry of Sindbis virus into vertebrate or invertebrate cells, the conformational changes occurring at low pH may mimic those occurring upon virus-receptor interaction. Here, we employed small-angle neutron scattering with contrast variation to probe how the structure of a mammalian-grown Sindbis virus responds to moderately acidic pH. Several changes took place throughout the virion structure when the pH decreased from 7.2 to 6.4. Specifically, the RNA in the virion core underwent a conformational change. Additionally, the protein was redistributed. A significant amount of protein moved from the layer containing the lipid bilayer to the exterior of the virion. The results improve our understanding of the pH-driven alteration of Sindbis virus structure.

Sindbis virus is the archetypal *Alphavirus*. It is composed of two concentric protein layers separated by a lipid bilayer. The inner core contains the nucleocapsid, which is comprised of the capsid protein condensed around the genomic plus-polarity single-stranded RNA. The glycoproteins E1 and E2, which are organized as heterotrimers, are embedded in the lipid bilayer, which is derived from the host cell. The outer and inner protein layers are anchored together through interactions of the glycoprotein E2 endodomain with the nucleocapsid core. As such, it is a relatively simple enveloped virus and an excellent model system for studies of structure and function.

Sindbis virus is an infectious molecular motor designed to deliver the genomic RNA to a suitable host cell for the purpose of virus propagation. Developing an understanding of the mechanism by which this macromolecular assembly delivers its infectious RNA cargo into the host cell has proven to be challenging. Two models of alphavirus infectivity have been proposed. One model proposes infection by endocytosis followed by fusion of the virus membrane with the membrane of the acidified endosome (22). The second model presents arguments for the direct penetration of the virus particle at the cell surface in the absence of endocytosis or acidification (25, 26, 33). In this model, the target cell membrane is breached by the formation of a pore that allows entry.

Both models postulate that conformational changes in the virus are important to the mechanism of infection. In the fusion model, the decrease in solution pH is the trigger that drives the particle to rearrange and expose the virus membrane for fusion and the release of the RNA into the cell cytoplasm. In the direct-penetration model, interactions of the virus glycoproteins with host receptors are proposed to trigger conformational changes, which may be the same as those induced by acidic pH, that open proteinaceous pores in the virus and the cell membrane through which the RNA can be extruded. A direct assay of pore formation in the presence of the Sindbis virus receptor is not as yet possible because the receptors have not been identified. The creation of pores during the infection process is suggested, however, by experiments demonstrating that the cell membrane becomes permeable to ions and small molecules as alphavirus entry takes place (27, 31, 38). Further research will be needed to resolve these issues.

Critical aspects of the structural analysis of Sindbis virus are its stability and its particle-to-PFU ratio of 1 (18). Several methodologies, including cryo-electron microscopy (cryo-EM) (33), X-ray crystallography (7), and neutralizing monoclonal antibody (MAb) binding (17), have been used to probe the structure of Sindbis virus exposed to low pH. Exposure of alphaviruses to acidic pH has a profound effect on the structure and function of the virion. Exposure of Sindbis virus attached to living cells to acidic pH can lead to cell-cell fusion if the cells are returned to neutral pH (6, 33). Fusion of the virus with protein-free, cholesterol-rich artificial membranes can occur with only exposure to acidic pH (23). Acidic pH irreversibly inactivates the virus and causes it to clump avian erythrocytes in the classic hemagglutination assay (2, 5). The erythrocytes, like living cells, are not fused under these circumstances. It is believed that the hemagglutination reaction results from the exposure of hydrophobic protein domains that subsequently adhere to cell lipid bilayers. The exposure of these buried domains causes the virus to clump, making morphological study of the virus at acidic pH, which establishes the conditions for infection, very difficult. Indeed, there is only one structure of an alphavirus that has been produced at the pH that induces hemagglutination (33). This structure reveals a massive and only partially reversible change in the surface and interior of the virus.

In the present study, small-angle neutron scattering (SANS) with contrast variation (12, 19) was used to investigate changes in the Sindbis virus structure after exposure to pH 6.4 that were

Received 14 October 2011 **Accepted** 26 November 2011
Published ahead of print 7 December 2011
Address correspondence to Dennis Brown, dennis_brown@ncsu.edu.
L. He and A. Piper contributed equally to this work.

doi:10.1128/JVI.06569-11

directly compared to measurements of the virus at pH 7.2. SANS with contrast variation has been successfully applied to the study of icosahedral viruses (1, 3, 4, 20, 21, 40), and the nondestructive nature of the neutrons does not result in a loss of infectivity (10). The use of contrast variation, in which the particles are measured in a series of H_2O-D_2O mixtures, makes it possible to determine how the lipid and RNA components of the virion interact with the proteins. The SANS data show an interesting movement of protein density that had been seen previously using cryo-EM. The SANS data, however, are the first to show how the lipid and RNA components of the virus interact with the virus proteins during the pH shift. As SANS is refined as a method for studying virus structure, these data will continue to provide invaluable information about the organization of these macromolecular particles and how they change during activation and infection.

MATERIALS AND METHODS

Virus production. Sindbis virus at pH 7.2 was produced and purified over two subsequent potassium tartrate gradients as described in our previous SANS study (10). Virus samples at pH 7.2 were prepared as a contrast series of 90%, 80%, 70%, 40%, 10%, and 0% D_2O. For the pH 6.4 samples, purified virus obtained from the second tartrate gradient was diluted 1:2 using phosphate-buffered saline (PBS) and loaded on a third step gradient comprised of a 35% to 76% step of glycerol in PBS (pH 7.2). The contrast series required fully hydrogenated and fully deuterated virus preparations. The virus eluted at 64% hydrogenated glycerol (in PBS made in H_2O) and at 34.6% deuterated glycerol (in PBS made in D_2O). To produce virus with pH 6.4, 1.0 M MOPS (morpholinepropanesulfonic acid) in 100% H_2O or 100% D_2O, pH 5.7, was added to a final concentration of 40 mM in the samples. Virus obtained from this protocol was deemed useable for SANS experiments at acidic pH with no particle aggregation. Contrast series samples with scattering-length densities (SLDs) equivalent to 100, 90, 75, 42, 15, and 0% D_2O were prepared by mixing fully hydrogenated and fully deuterated virus preparations in appropriate proportions. We note that the pHs of all deuterated buffers were corrected and adjusted to 7.2 or 6.4 according to the following formula: $pD = pH_{meas} + 0.4$ (29). This ensured that all samples within a series had the same pH. Here, we use pH when referring to the solutions regardless of their D_2O content to avoid confusion.

SANS measurements. The SANS experiments were carried out at HFIR Bio-SANS (CG3), Oak Ridge National Laboratory (30). A detailed description of the instrument and its various components can be found in reference 30. Samples were measured at room temperature in sealed, 1-mm-path-length quartz cuvettes at pH 7.2 and pH 6.4. The concentrations of the samples were ~500 μg/ml. The neutron wavelength for all measurements was set to 6 Å with a wavelength spread, $\Delta\lambda/\lambda$, of 0.14. Data were collected on three occasions. Contrast variation series SANS data at pH 7.2 were detected with a 1- by 1-m^2 ^{3}He-filled, two-dimensional, position-sensitive detector with 192 by 192 pixels (Ordela, Inc., Oak Ridge, TN) using a single sample-to-detector distance of 6.8 m, providing a q range between a q_{min} of 0.006 $Å^{-1}$ and a q_{max} of 0.16 $Å^{-1}$. Additional SANS data for the two pH conditions in 100% D_2O were collected for model-independent analysis at a later date using two sample-to-detector distances (15.3 m and 6.8 m) that provided a q range from a q_{min} of 0.003 $Å^{-1}$ to a q_{max} of 0.16 $Å^{-1}$. The contrast variation series data from the samples at pH 6.4 were collected with a 40-cm by 40-cm ^{3}He-filled two-dimensional (2D) detector with 128 by 128 pixels (Ordela, Inc., Oak Ridge, TN). Two sample-to-detector distances (15.3 m and 2.5 m) were used to cover a q range between a q_{min} of 0.003 $Å^{-1}$ and a q_{max} of 0.16 $Å^{-1}$ for the pH 6.4 data. In all cases, the samples and corresponding buffers were collected for approximately 3 h at each detector setting to obtain acceptable counting statistics. The raw 2D data were corrected for the detector pixel response and dark current, which represent the ambient radiation background and electronic noise, before being azimuthally averaged to produce the 1D scattered intensity profile $I(q)$ versus q, where q is equal to $4\pi \sin\theta/\lambda$ and 2θ is the scattering angle. Data were placed on an absolute scale (cm^{-1}) through the use of calibrated standards (39). The reduced 1D profiles from the two detector distances employed at pH 6.4 were merged by manually scaling the high-q data to the low-q data because of the very different instrument resolution functions of the two configurations employed, while the two samples measured in 100% D_2O were merged using software developed by the National Institutes of Standards and Technology (24). The final reduced data were produced by subtracting the $I(q)$ for the buffer from that of the sample and including a constant to account for the difference in incoherent scattering that arises from the difference in hydrogen content that results from the displacement of buffer by the virus in the sample.

SANS data analysis. Data collected for the two pH conditions in 100% D_2O were subjected to three different model-independent analyses. The data were analyzed according to the method of Guinier and Fournet for the radius of gyration, R_g (8). R_g is a model-independent parameter that provides a measure of the compactness of a particle. Guinier analysis utilizes a series expansion of $I(q)$ to derive an approximate Gaussian form for the intensity.

$$I(q) \propto I(0)\exp(-q^2R_g^2/3) \quad (1)$$

A linear fit of $\ln(I(q))$ versus q^2 provides the intercept and slope, which are related to the zero-angle scattering intensity, $I(0)$, and R_g, respectively. The expansion used to derive the Guinier approximation is applicable to only a limited range of low q values. For a nearly spherical particle, such as Sindbis virus, the approximation is valid for a $q \times R_g$ value of <1.3 (35).

The second model-independent analysis applied to the SANS data was to determine the excess radial-scattering-length distribution function. For a spherically symmetric particle, the scattering-length density relative to that of the solvent can be determined by performing a Fourier transform of the structure factor, $F(q)$, through equation 2.

$$\rho(r) - \rho_s = \frac{1}{2\pi r}\int_0^\infty q \cdot F(q) \cdot \sin(qr) \cdot dq \quad (2)$$

$F(q)$ is related to scattering intensity as follows: $I(q) = |F(q)|^2$. While the intensity is strictly a positive number, it is possible for $F(q)$ to be either positive or negative. $F(q)$ is a continuous function; therefore, the sign alternates from positive to negative smoothly. It was assigned to alternate after each sharp minimum in the measured profile. Previous researchers found that $\rho(r) - \rho_s$ is not reliable at short distances due to truncation errors that result from performing a Fourier transform over a limited q range and structural deviations from true spherical symmetry (3, 21). Here, the entire measured q range was used for the Fourier transform. The direct transformation of the data into $\rho(r) - \rho_s$ prevented taking the instrument resolution into account.

Data collected for the Sindbis virus in 100% D_2O were also fitted for the distance distribution function, $P(r)$, which is the frequency of all pairwise distances within a scattering particle weighted by the scattering-length density difference relative to the solvent, $P(r)$. $P(r)$ is related to $I(q)$ through equation 3.

$$P(r) = \frac{1}{2\pi^2}\int_0^\infty qr \cdot I(q) \cdot \sin(qr) \cdot dq \quad (3)$$

$P(r)$ was evaluated using GNOM, which employs an indirect Fourier transform method (34). The instrument resolution effects, which result from the sizes of the apertures, their separation, and the $\Delta\lambda/\lambda$ value used, were accounted for during the fitting. The data collected at both detector distances were fitted simultaneously. The maximum linear dimension of the scattering particle, D_{max}, is provided by the fitting. The second moment of $P(r)$, which is equal to the square of the R_g of the particle, is also output by GNOM.

A multishell spherical model was also applied to the contrast variation series data to better understand the radial distribution of material in the virus. While the Sindbis virus is known to be an icosahedral particle, EM studies suggest that the particle has a strongly spherical character, making

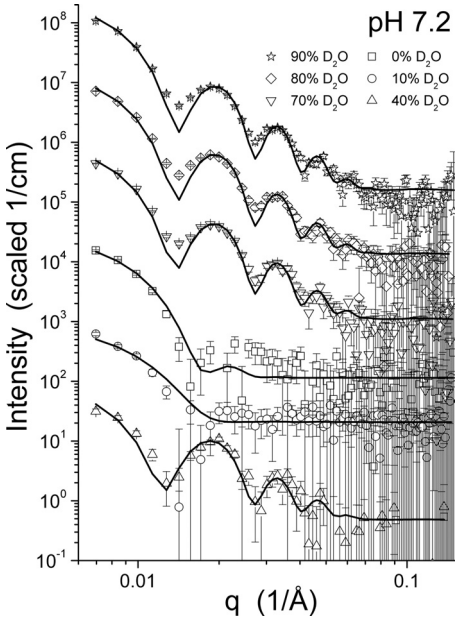

FIG 1 SANS contrast variation series data for Sindbis virus BHK at pH 7.2. The curves have been offset for clarity. The solid lines are the best fit model intensity profiles determined as described in Materials and Methods. The error bars indicate experimental uncertainties in the data.

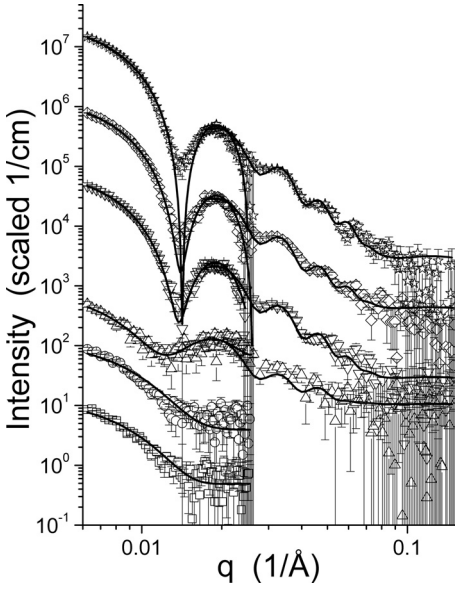

FIG 2 SANS contrast variation series data for Sindbis virus BHK at pH 6.4. The curves have been offset for clarity. The high-q data for the two data sets are not shown and were eliminated from the fitting because they were not of sufficient statistical quality. The solid lines are the best fit model intensity profiles determined as described in Materials and Methods. The error bars indicate experimental uncertainties in the data.

it reasonable to model the structure of the virus with concentric spherical shells. The intensity profile of the multishell model is given by equation 4.

$$I(q) = A\frac{\phi}{V_p}\left[\sum_{i=1}^{N}\frac{3V_i(\rho_i - \rho_{i+1})j_1(qr_i)}{qr_i}\right]^2 + bkg \quad (4)$$

The volume fraction of the particles in solution is ϕ, V_p is the volume of the virus particle, and V_i and r_i are the volume and radius of the ith concentric sphere, respectively. N is the number of shells used. The spherical Bessel function is given by the following equation: $j_1(x) = (\sin x - x \cos x)/x^2$. The A in equation 5 is a relative scale factor, while bkg is an additive constant background.

The scattering-length density of the ith shell was determined by assigning volumes of the known contents of the virus to the various shells, as shown in equation 5.

$$\rho_i = \frac{1}{V_i}\left[V_{i,\text{lipid}}\,\rho_{\text{lipid}} + V_{i,\text{protein}}\,\rho_{\text{protein}} + V_{i,\text{RNA}}\,\rho_{\text{RNA}} + (V_i - V_{i,\text{lipid}} - V_{i,\text{protein}} - V_{i,\text{RNA}})\rho_{\text{solvent}}\right] \quad (5)$$

In equation 5, V_i, $V_{i,\text{lipid}}$, $V_{i,\text{protein}}$, and $V_{i,\text{RNA}}$ are the volumes of the shell and the volumes of protein, lipid, and RNA assigned to the shell, respectively. The scattering-length densities of the solvent, ρ_{solvent}, and individual components, ρ_{lipid}, ρ_{protein}, and ρ_{RNA}, were calculated from the composition of the materials and the fraction of D_2O in the solvent, as determined from the transmission (13, 14). The scattering intensities in the contrast series were then calculated from the model using equation 4 and compared to the entire contrast variation series of data simultaneously using the reduced χ^2, as described previously (11, 37). To efficiently search the potential parameter space, a Monte Carlo search was employed. The radii of the four shells were variables, as were the volumes of protein, lipid, and RNA assigned to each shell. Constraints were applied to the volumes of material assigned to each shell. In addition to not allowing more material to be assigned to a shell than the volume of the shell allowed, the total volume of each material in the model was constrained to values estimated from previous studies (33). Each successive shell filled could be assigned only up to the amount of material remaining. Further constraints were applied that were loosely based on the organization of the virus determined by cryo-EM (9, 32, 41). Specifically, all of the lipid was assigned to the third shell. The innermost shell, or core, contained only RNA and solvent. As a result, the protein was allowed to reside only in the outer three shells. RNA was restricted to lie within the first two shells of the structure. Additionally, if less than 10% of the total possible volume of a given material was selected by the Monte Carlo process, the actual volume assigned was set to zero. Over 15 million models were tested during the fitting of each of the pH 7.2 and pH 6.4 contrast variation series data. The variability of the results of the modeling was characterized as described previously (11).

RESULTS

The contrast variation series data collected at pH 7.2 and 6.4 are shown in Fig. 1 and 2, respectively. The data quality strongly depend on the contrast between the virus and the solution. The samples measured in solutions with low D_2O content have the weakest signal, consistent with the amount of lipid in the virion, which has a scattering-length density close to that of the low-D_2O-content solutions. Only the low-q data from the two samples measured in 0% D_2O and 4% D_2O at pH 6.4 were suitable for analysis and the modeling employed as a result of the limited availability of beam time. The data sets collected in solutions having high D_2O content show multiple oscillations consistent with a particle having a strongly spherical character.

Guinier fits performed on data sets collected in high D_2O content are shown in Fig. 3. At pH 7.2, the Sindbis virus particle has an R_g of 258.9 ± 2.3 Å, while it has an R_g of 242.6 ± 2.5 Å at pH 6.4. The Guinier plots show subtle signs of high-molecular-weight contaminants, which may be virion aggregates, that can be seen as the subtle change in the slope of the data seen at the lowest q. As a result, data below a q of 0.006 $Å^{-1}$ were not used for the data analysis and modeling.

The $P(r)$ values derived from the data used for the Guinier

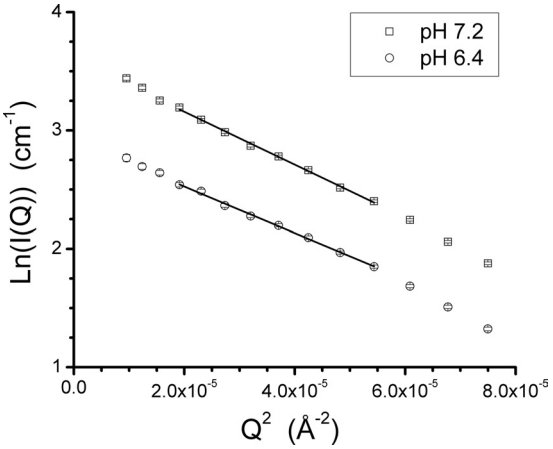

FIG 3 Guinier analysis of Sindbis virus BHK at pH 7.2 and 6.4.

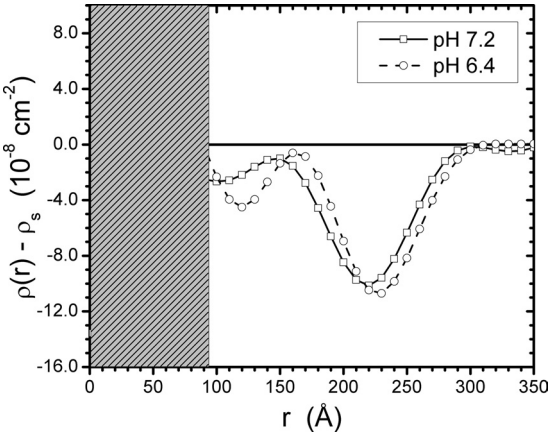

FIG 5 Radial-scattering distribution function for BHK at pH 7.2 and 6.4. The shading indicates the radii where the curves are not considered reliable.

analysis are shown in Fig. 4, while the $\rho(r) - \rho_s$ values determined from the same data are shown in Fig. 5. The $P(r)$ value shows a redistribution of mass within the particle when the pH decreases. At pH 7.2, the curve shows a main peak near 380 Å with a shoulder near 300 Å. At pH 6.4, the peak at lower vector lengths increases in amplitude without moving considerably, but the peak at higher vector lengths moves 20 Å to longer distances with a resulting redistribution of mass to longer vector lengths. These changes are echoed in the $\rho(r) - \rho_s$ curves. The main feature in both curves derived from the data is a strong minimum, previously identified as the lipid layer (10), that is centered at ~220 Å at pH 7.2 and ~230 Å at pH 6.4. There is also an increase in material between 100 and 160 Å at pH 6.4. These curves, being derived by directly transforming the SANS data, are not considered reliable at short vector lengths, which are shaded in Fig. 5.

The results of the 4-shell fitting by assigning the protein, lipid, and RNA to the shells against the SANS contrast variation series data collected for the Sindbis virus at pH 7.2 and pH 6.4 are presented in Table 1. The fits to the data at pH 7.2 are shown in Fig. 1, while the fits to the SANS data collected at pH 6.4 are shown in Fig. 2. The model profiles collected at pH 7.2 have a χ^2 value of 8.08 to the SANS data, while χ^2 is 2.68 for the model fit to the pH 6.4 data. The qualities of the fits, as can be seen in the figures, are comparable, and the differences in the χ^2 value can be attributed to the different statistical quality of the data sets at the various contrast values measured and the relative numbers of data points. The difference can also be partially attributed to the removal of the noisy high-q data from the two data sets at pH 6.4. The structural parameters of the best fit structures summarized in Table 1 show a redistribution of material in the virus as the pH is lowered from 7.2 to 6.4. In the innermost two shells, which correspond to the core and nucleoprotein capsid, there is a subtle redistribution of RNA. Shell 1, the core of the Sindbis virion, shrinks and fills with RNA by excluding solvent, while the volume of RNA in shell 2 is unchanged. The volume of shell 2 increases as a result of the decrease in its inner radius and increase in the outer radius. The amount of protein in the shell increases significantly over that found at pH 7.2. Shell 3, where the lipid was constrained to lie, undergoes a subtle change in the inner radius without a change in the outer radius. More interestingly, the amount of protein in this shell dramatically decreases from over half of the available protein at pH 7.2 to virtually none at pH 6.4. This transition in the protein content of shell 3 is accompanied by a large increase in the amount of protein in the outermost shell that corresponds to the glycoprotein coat of the Sindbis virus. The radius of the outermost shell also increases as the pH decreases from 7.2 to 6.4.

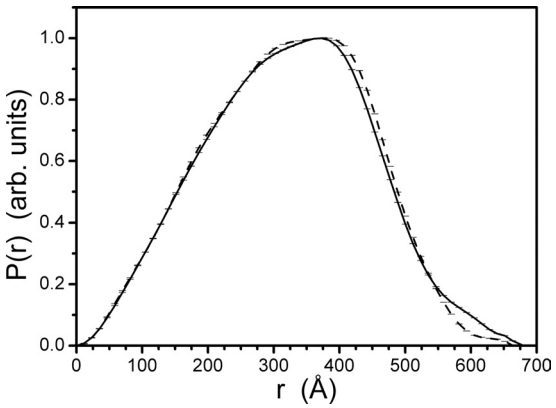

FIG 4 Pair distance distribution function for BHK at pH 7.2 (solid line) and 6.4 (dashed line). arb., arbitrary.

DISCUSSION

Neutron-scattering data for the Sindbis virion support the findings of previous studies on the conformational changes that this macromolecular structure undergoes when triggered by changes in certain external environmental conditions. In addition to low pH (5.3), heat and neutralizing MAb binding can induce conformational rearrangements of the particle (17). In each case, induction of these altered conformations leads to inactivation of the virus. Through the use of SANS with contrast variation of virus treated at pH 7.2 and 6.4, a glimpse of the participation of the lipid and RNA components with the proteins has been revealed. The only shell that is essentially unchanged with respect to volume is the lipid shell. At pH 6.4, the RNA is found in shell 1 with significantly reduced volume and solvent content. While the RNA content of shell 2 does not change in response to pH 6.4, there is a significant shift in the amount of protein occupying the shell from that seen at pH 7.2 (Table 1). This shift in density suggests reorganization of the RNA-protein contacts, which are proposed to

TABLE 1 Results of 4-shell models filled by material volumes for Sindbis virus at pH 7.2 and pH 6.4

Shell	pH	Radius (Å)	Vol (10^6 Å^3)				
			Total	Protein	Lipid	RNA	Solvent
1	7.2	74.0 ± 3.2	1.70 ± 0.23	0.00[a]	0.00[a]	0.27 ± 0.20	1.43 ± 0.28
	6.4	46.8 ± 5.2	0.44 ± 0.16	0.00[a]	0.00[a]	0.30 ± 0.09	0.14 ± 0.10
2	7.2	199.7 ± 2.5	32.94 ± 1.24	5.15 ± 0.55	0.00[a]	3.00 ± 0.09	24.80 ± 0.87
	6.4	192.8 ± 1.9	28.33 ± 0.86	3.53 ± 0.41	0.00[a]	3.03 ± 0.20	21.77 ± 0.61
3	7.2	270.3 ± 2.1	52.75 ± 2.42	5.96 ± 1.26	22.00[a]	0.00[a]	24.80 ± 1.39
	6.4	270.35 ± 2.3	49.39 ± 2.70	0.81 ± 0.74	22.00[a]	0.00[a]	26.58 ± 2.22
4	7.2	337.8 ± 12.5	79.38 ± 18.05	1.61 ± 1.28	0.00[a]	0.00[a]	77.77 ± 18.69
	6.4	360.3 ± 13.9	114.06 ± 21.00	5.14 ± 0.78	0.00[a]	0.00[a]	108.93 ± 21.22

[a] Value fixed by a constraint applied during the Monte Carlo search (see Materials and Methods).

accompany infection. This RNA-protein organization would need to be reversible or not detrimental to infectivity, since pH 6.4 does not abrogate infectivity, nor does it establish conditions for hemagglutination or cell membrane fusion when returned to neutral pH (6). It is of significant interest that such a large volume of protein shifts from shells 2 and 3 into the outermost shell 4. It was unexpected that protein would be displaced from the lipid (shell 3) at pH 6.4. This result suggests that large conformational and spatial reorganization of the glycoproteins occurs.

The cryo-EM reconstruction of Sindbis virus at pH 5.3 (33) also shows large conformational changes of the glycoprotein coat of the virus particle. Exposure of virus to pH 5.3 results in a loss of infectivity that is not restored on return to neutral pH, which is thought to result from irreversible conformational changes. In the adjacent shell 3, the SANS data show that although the lipid shell volume does not change, there is a significant redistribution of the protein content of this shell at pH 6.4. For this to be possible, the protein domains contained in the lipid shell must be sufficiently flexible to allow them to physically shift from the lipid to occupy space in the adjacent shell. Previous work on the functions of the protein domains that occupy the lipid shell, the transmembrane domains (TMD), suggested that amino acid residues located at the carboxyl terminus of the TMD of glycoprotein E2 have dual functionality (15, 16). The TMD can function in the lipid shell or in the endodomain (a component of shell 2), depending on the lipid shell composition. In the present work, the lipid composition is not a variable, and a shift in the protein occupancy of the lipid shell could alternatively be explained by a reorientation of the proposed TMD tilt or by an increased hydrophobic mismatch with the lipid. If conformational changes in the helical TMD occur at pH 6.4, conformational reversibility is required, because infectivity is conserved. The SANS data strongly suggest that these TMD must also respond to these large conformational switches. Redistribution of protein from the lipid shell into the outer shell 4, the ectodomain, was not determined previously by cryo-EM (33). The pH series used in the cryo-EM studies, which is the only technique capable of studying the Sindbis virion structure at pH 5.3, also demonstrated that low-pH treatment of Sindbis virions resulted in an increase in the particle radius due to the induction of large conformational changes on all surfaces of the outer protein shell (33), which is supported by the SANS data.

Conclusions. SANS is a well-established, nondestructive, powerful tool for studying virus structure in dilute solution (1, 3, 4, 10, 20, 21, 40). The method of modeling the data employed here has afforded new insight into the structural changes that take place in the various components of Sindbis virus when the pH is decreased from 7.2 to 6.4. Although in a few cases information has been obtained regarding the organization of virus RNA by X-ray crystallography (28, 36), almost no information exists for that organization in the alphaviruses. There is also no information on how the organization changes upon virus activation. The use of models built on the distribution of the materials that make up virions has the potential to be a boon for the field of virology.

ACKNOWLEDGMENTS

Research was sponsored by the Laboratory Directed Research and Development Program of Oak Ridge National Laboratory (ORNL).

D.T.B. and R.H. are supported by The Foundation for Research, Carson City, NV. This research at Oak Ridge National Laboratory's Center for Structural Molecular Biology (FWP ERKP291) was supported by the Office of Biological and Environmental Research, using facilities supported by the U.S. Department of Energy, managed by UT-Battelle, LLC, under contract no. DE-AC05-00OR22725.

REFERENCES

1. **Aramayo R, et al.** 2005. Divalent ion-dependent swelling of tomato bushy stunt virus: a multi-approach study. Biochim. Biophys. Acta **1724**:345–354.
2. **Burge BW, Huang AS.** 1970. Comparison of membrane protein glycopeptides of Sindbis virus and vesicular stomatitis virus. J. Virol. **6**:176–182.
3. **Chauvin C, Witz J, Jacrot B.** 1978. Structure of tomato bushy stunt virus—model for protein-RNA interaction. J. Mol. Biol. **124**:641–651.
4. **Cusack S, Ruigrok RWH, Krygsman PCJ, Mellema JE.** 1985. Structure and composition of influenza-virus—a small-angle neutron-scattering study. J. Mol. Biol. **186**:565–582.
5. **Dalrymple JM, Schlesinger S, Russell PK.** 1976. Antigenic characterization of two sindbis envelope glycoproteins separated by isoelectric focusing. Virology **69**:93–103.
6. **Edwards J, Brown DT.** 1986. Sindbis virus-mediated cell fusion from without is a two-step event. J. Gen. Virol. **67**:377–380.
7. **Gibbons DL, et al.** 2004. Purification and crystallization reveal two types of interactions of the fusion protein homotrimer of Semliki Forest virus. J. Virol. **78**:3514–3523.
8. **Guinier A, Fournet G.** 1955. Small-angle Scattering of X-rays. Wiley, New York, NY.
9. **Harrison SC, David A, Jumblatt J, Darnell JE.** 1971. Lipid and protein organization in Sindbis virus. J. Mol. Biol. **60**:523.
10. **He LL, et al.** 2010. The structure of Sindbis virus produced from vertebrate and invertebrate hosts as determined by small-angle neutron scattering. J. Virol. **84**:5270–5276.
11. **Heller WT.** 2006. ELLSTAT: shape modeling for solution small-angle scattering of proteins and protein complexes with automated statistical characterization. J. Appl. Crystallogr. **39**:671–675.
12. **Heller WT.** 2010. Small-angle neutron scattering and contrast variation: a powerful combination for studying biological structures. Acta Crystallogr. D **66**:1213–1217.

13. **Heller WT, et al.** 2003. Small-angle neutron scattering with contrast variation reveals spatial relationships between the three subunits in the ternary cardiac troponin complex and the effects of troponin I phosphorylation. Biochemistry **42**:7790–7800.
14. **Heller WT, et al.** 2004. C subunits binding to the protein kinase A RI alpha dimer induce a large conformational change. J. Biol. Chem. **279**: 19084–19090.
15. **Hernandez R, Ferreira D, Sinodis C, Litton K, Brown DT.** 2005. Single amino acid insertions at the junction of the Sindbis virus E2 transmembrane domain and endodomain disrupt virus envelopment and alter infectivity. J. Virol. **79**:7682–7697.
16. **Hernandez R, Lee H, Nelson C, Brown DT.** 2000. A single deletion in the membrane-proximal region of the Sindbis virus glycoprotein E2 endodomain blocks virus assembly. J. Virol. **74**:4220–4228.
17. **Hernandez R, Paredes A, Brown DT.** 2008. Sindbis virus conformational changes induced by a neutralizing anti-E1 monoclonal antibody. J. Virol. **82**:5750–5760.
18. **Hernandez R, et al.** 2003. Deletions in the transmembrane domain of a Sindbis virus glycoprotein alter virus infectivity, stability, and host range. J. Virol. **77**:12710–12719.
19. **Ibel K, Stuhrmann HB.** 1975. Comparison of neutron and X-ray-scattering of dilute myoglobin solutions. J. Mol. Biol. **93**:255–265.
20. **Inoue H, Timmins PA.** 1985. The structure of rice dwarf virus determined by small-angle neutron-scattering measurements. Virology **147**: 214–216.
21. **Jacrot B, Chauvin C, Witz J.** 1977. Comparative neutron small-angle scattering study of small spherical RNA viruses. Nature **266**:417–421.
22. **Kielian M.** 1995. Membrane fusion and the alphavirus life cycle. Adv. Virus Res. **45**:113–151.
23. **Kielian MC, Helenius A.** 1984. Role of cholesterol in fusion of Semliki Forest virus with membranes. J. Virol. **52**:281–283.
24. **Kline SR.** 2006. Reduction and analysis of SANS and USANS data using IGOR Pro. J. Appl. Crystallogr. **39**:895–900.
25. **Kononchik JP, Jr, Hernandez R, Brown DT.** 2011. An alternative pathway for alphavirus entry. Virol. J. **8**:304.
26. **Kononchik JP, Vancini R, Brown DT.** 2011. Alphavirus adsorption to mosquito cells as viewed by freeze fracture immunolabeling. Virology **415**: 132–140.
27. **Koschinski A, Wengler G, Repp H.** 2005. Rare earth ions block the ion pores generated by the class II fusion proteins of alphaviruses and allow analysis of the biological functions of these pores. J. Gen. Virol. **86**:3311–3320.
28. **Lane SW, et al.** 2011. Construction and crystal structure of recombinant STNV capsids. J. Mol. Biol. **413**:41–50.
29. **Lumry R, Smith EL, Glantz RR.** 1951. Kinetics of carboxypeptidase action. 1. Effect of various extrinsic factors on kinetic parameters. J. Am. Chem. Soc. **73**:4330–4340.
30. **Lynn GW, et al.** 2006. Bio-SANS: a dedicated facility for neutron structural biology at Oak Ridge national laboratory. Physica B **385–386**:880–882.
31. **Madan V, Sanz MA, Carrasco L.** 2005. Requirement of the vesicular system for membrane permeabilization by Sindbis virus. Virology **332**: 307–315.
32. **Paredes AM, et al.** 1993. 3-Dimensional structure of a membrane-containing virus. Proc. Natl. Acad. Sci. U. S. A. **90**:9095–9099.
33. **Paredes AM, et al.** 2004. Conformational changes in Sindbis virions resulting from exposure to low pH and interactions with cells suggest that cell penetration may occur at the cell surface in the absence of membrane fusion. Virology **324**:373–386.
34. **Semenyuk AV, Svergun DI.** 1991. GNOM: a program package for small-angle scattering data-processing. J. Appl. Crystallogr. **24**:537–540.
35. **Svergun DI, Koch MHJ.** 2003. Small-angle scattering studies of biological macromolecules in solution. Rep. Prog. Phys. **66**:1735–1782.
36. **Tang L, et al.** 2001. The structure of pariacoto virus reveals a dodecahedral cage of duplex RNA. Nat. Struct. Biol. **8**:77–83.
37. **Tjioe E, Heller WT.** 2007. ORNL_SAS: software for calculation of small-angle scattering intensities of proteins and protein complexes. J. Appl. Crystallogr. **40**:782–785.
38. **Wengler G, Koschinski A, Dreyer F.** 2003. Entry of alphaviruses at the plasma membrane converts the viral surface proteins into an ion-permeable pore that can be detected by electrophysiological analyses of whole-cell membrane currents. J. Gen. Virol. **84**:173–181.
39. **Wignall GD, Bates FS.** 1987. Absolute calibration of small-angle neutron-scattering data. J. Appl. Crystallogr. **20**:28–40.
40. **Witz J, Timmins PA, Adrian M.** 1993. Organization of turnip yellow mosaic-virus investigated by neutron small-angle scattering at 80-K: an intermediate state preceding decapsidation of the virion. Proteins **17**:223–231.
41. **Zhang W, et al.** 2002. Placement of the structural proteins in Sindbis virus. J. Virol. **76**:11645–11658.